J Mater Sci (2023) 58:11748–11760

Electronic materials

Fluorinated carbon nanotubes: a low-cost hole transport layer for perovskite solar cells

Mustafa K. A. Mohammed[1,*], Ali K. Al-Mousoi[2], Anjan Kumar[3], Abdul Rasool J. Katae[4], Omar A. Khaleel[4], Duha S. Ahmed[4], and M. Khalid Hossain[5]

[1] University of Warith Al-Anbiyaa, Karbala 56001, Iraq
[2] Department of Radiology and Ultrasonography Techniques, College of Medical Techniques, Al-Farahidi University, Baghdad 10011, Iraq
[3] Department of Electronics and Communication Engineering, GLA University, Mathura 281406, India
[4] Applied Sciences Department, University of Technology-Iraq, Baghdad 10011, Iraq
[5] Institute of Electronics, Atomic Energy Research Establishment, Bangladesh Atomic Energy Commission, Dhaka 1349, Bangladesh

Received: 15 March 2023
Accepted: 20 June 2023
Published online: 14 July 2023

ABSTRACT

The employment of cost-effective and durable structures is essential for the successful commercialization of perovskite solar cells (PSCs). Identifying a viable substitute for hole-selective materials (HSMs), which represent a significant expense in the production of PSCs, could provide a number of benefits. Carbon nanotube-based PSCs have shown promising potential as an alternative to conventional PSCs due to their unique properties such as excellent stability behavior to be potential for commercialization to produce green energy for human industries. One of the most crucial disadvantages of carbon derivatives as HSMs in CPSCs is their low hole mobility, which in the current study has been targeted. In the current study, to increase the efficiency of CPSCs, net carbon nanotubes (CNTs) were doped with nonmetallic fluorine via a facile synthesis method. It was found that introducing fluorine-doped CNTs (F-CNTs) as HSM for $MAPbI_3$ perovskite could reach up to an efficiency of 15.29%, higher than the efficiency of 13.70% in devices with a net CNT layer. By doping CNTs with fluorine, the charge-transfer resistance and series resistance are reduced, resulting in lower charge recombination at the perovskite/CNT interface Also, the CPSCs with F-CNT film were more stable in ambient air because the F-CNTs covered more of the perovskite layer. The future trend of CNT-based PSCs is expected to focus on improving their performance, and exploring their potential for various optoelectronics.

Handling Editor: Kevin Jones.

Mustafa K. A. Mohammed and Duha S. Ahmed have contributed equally.

Address correspondence to E-mail: mustafa_kareem97@yahoo.com

https://doi.org/10.1007/s10853-023-08756-1

Introduction

Solar cells offer clean energy and an alternative to burning fossil fuels; however, recently, photovoltaics based on halide perovskites have surpassed those based on crystalline silicon photovoltaics in popularity due to their low cost, versatility, and superior energy conversion efficiency [1–5]. Perovskite-based photovoltaic devices have a high-performance rate due to a variety of characteristics, including but not limited to their high absorption coefficient, long carrier diffusion lengths, readily adjustable band gaps, and high carrier mobility [6–12]. Using a maximum output efficiency that is more than 25%, perovskite solar cells that are manufactured with metal halide appear to be a significant advancement over earlier generations [1]. Despite this advancement, a lot more work has to be done to make PSC inexpensive, stable, and have greater conversion efficiency. The cost-effectiveness of a material utilized as a charge transport layer in PSCs can be determined through various factors such as the cost of starting materials, the ease of processing, and the overall performance of the photovoltaic. One critical component of a perovskite solar cell is the hole-selective material (HSM), which plays a key role in extracting charge carriers from the perovskite layer and transporting them to the electrode. In perovskite solar cells, Spiro-OMeTAD material is commonly used as a HSM, which increases the final price of PSCs. Unfortunately, due to its high cost of synthesis, instability, and need of dopants because of low hole mobility, the use of Spiro-OMeTAD has been encountered a drawback [13–15]. To solve these obstacles, in addition to reducing cell cost and overall stability of the PSCs, the application of stable and available materials with a facile preparation is suggested. Carbon derivatives includes carbon black, graphene, graphite/amorphous carbon, and CNTs suggest low cost, high conductivity, eventual low-temperature processing, chemical stability and environmental kindness materials for using as HSM in PSCs [16–19]. Accordingly, researchers have focused their attention on carbon nanotubes (also known as CNTs), which possess exceptional electrical and optical characteristics and have the potential to bring about the needed improvement [20–24]. In conventional devices using CPSCs, the perovskite active film is placed between two charge-selective materials, one of which is an electron-selective material (ESM), and the other is a hole-selective material (HSM) [25–28]. Early CPSC-based solar cells commonly use Spiro-OMeTAD and titanium dioxide as HSM and ESM, respectively. CNTs were investigated as a hole transport material as well as a contact electrode as an alternative to traditional p-type hole transport materials such as Spiro-OMeTAD and poly(bis(4-phenyl)(2,4,6-trimethylphenyl) amine (PTAA) due to their high charge carrier mobility and long-range transport [29–33]. The carbon nanotube was included in the design of the cell since there is a possibility that it may slow down the crystallization dynamics of the perovskite layer [23, 24, 33, 34]. In addition, carbon nanotubes have the potential to act as an ion blocker, preventing the passage of iodide into the metal halide perovskite absorber, and so significantly extending the stability of the CPSCs [35]. Despite being used as a hole-selective material, single-walled CNTs (SWCNTs) are not sufficiently charge selective for light-generated holes and cannot provide a strong field to avoid interfacial recombination losses; as a result, a low photogenerated voltage is produced [24, 33, 36]. For this reason, multi-walled CNTs (MWCNTs) were used in this study since their inner walls would remain unharmed and conductive even if their outer nanotube walls reacted with their immediate surroundings [37]. However, CPSCs that use pure CNTs as an HSM often exhibit subpar results due to a misaligned energy level alignment and the fact that the Femi levels of pure CNTs are much higher than those of perovskite [38, 39]. This reduces the charge transport rate and diminishes the V_{OC}. In addition, since the pure-CNT coating has poor conductivity, the fabricated solar cells suffer from poor hole transport behavior. The capacity to alter the hole extraction and transfer abilities of MWCNTs can be manipulated using a number of different tactics, one of the most successful of which is the elemental doping approach. Researchers led by Yang have shown that enhancing the amount of boron doping in MWNTs greatly improves the charge extraction capabilities in CPSCs compared to the untreated ones [40]. The CPSC obtained an impressive conversion efficiency of 15.2% using boron-doped MWNTs. Using $CsPbI_2Br$ as the perovskite material and a P3HT-MWCNT hybrid as the HSM, Wang and colleagues created a CPSC that is both stable and efficient [41]. By acting as a barrier between the $CsPbI_2Br$ layer and the surrounding air,

the compact P3HT-MWCNT film considerably improves the layer's stability. This group was able to stabilize device efficiency at 8.85% and exhibit good stability by maintaining 85% of their original value for more than 240 h at room temperature. For better carrier mobility and conductivity, Seunghyun Baik and colleagues used multi-walled carbon nanotubes in Spiro-OMeTAD [42]. To prevent unwanted back-electron transport and make full use of the superior charge transport afforded by Spiro-OMeTAD/MWNTs, a hybrid including both Spiro-OMeTAD/MWNTs and pure Spiro-OMeTAD was developed. This group achieved a conversion efficiency above 15% by controlling the MWNT concentration. Kazunari Matsuda and his team proved that the addition of a buffer layer composed of graphene oxide and single-walled CNTs results in a remarkable increase in the overall cell performance of metal halide PSCs [25]. The buffer layer composed of CNTs and graphene oxide functions as an effective HSM. Because of the complementary characteristics of carbon nanotubes and graphene oxide, an energy conversion efficiency of above 13% was attained in a $MAPbI_3$-based perovskite solar cell. An MWCNT electrode was employed in the HSL-free carbon-based PSC by Shihe Yang and colleagues [30]. The higher performance may be attributed to the hole transport pathway that is located at the interface of MWCNTs and perovskites. Following some initial tweaking, they were able to attain a performance of 12.7% and a very remarkable fill factor of 80%. Shuhui Yin and his colleagues used CNTs and carbon fiber as counter electrodes for HSL-free perovskite solar cells [20]. It was discovered that CNTs/carbon fiber material significantly improved the contact area between the perovskite and carbon layers, reducing charge-transfer resistance and enhancing hole extraction capability at the perovskite electrode interface. This group achieved a conversion efficiency of 11.8%.

In view of the well-defined morphology, nanosize, and high surface area of CNT, fluorine-modified CNTs (F-CNTs) with varying F ratios were simply prepared and used as hole transport layers for carbon-based PSCs. The MWCNTs have a F-rich surface, while the intact CNT inner walls provide efficient hole transportation from perovskite to the back electrodes. By incorporating CNTs in between the $MAPbI_3$ film and electrode, CNTs were partially embedded into the perovskite film, acting as a hole extraction and transfer pathway between them. The CPSC performance and influences of F doping on PCE and ambient stability were elucidated through material characterizations and the current density–voltage (*J-V*) test. The CNT bridge approach provides an intimate $MAPbI_3$/CNT interface, leading to a champion efficiency of 15.29% with an FF of 79.05%. The unencapsulated cells showed excellent stability under environmental conditions for 100 days when they were maintained in the dark.

Experiments

Functionalization of carbon nanotubes

Pristine CNTs with properties of 99 wt% purity, with 8 nm diameter, and 50–200 nm lengths, were bought from the SkySpring Nanomaterials, Inc., USA, and used as received. To prepare the functionalized CNTs, the CNTs and the acids mixture (sulphuric and nitric acids) in a volume (v/v) ratio of 3:1, were used. To 100 mg of pristine CNTs, a mixture of concentrated sulphuric (95%) and nitric acids (65%), which were obtained from J. T. Baker Company, and Central Drug House, England, respectively, were used. The resulting concoction was ultrasonically vibrated for 30 min before being diluted with distilled water, vacuum filtered through a cellulose nitrate membrane (0.22 μm), and baked at 110 °C overnight [43].

Solution preparation

5 mL of ethyl alcohol (EtOH, 99.8%, Merck), 35 μL of 2 M hydrochloric acid (HCl, 37%, Merck), and 350 μL of titanium tetraisopropoxide (TTIP, 99.99%, Sigma-Aldrich) were mixed through vigorous stirring for 30 min at 0 °C. The obtained solution was used as a compact titanium oxide (c-TiO_2) precursor. To prepare a mesoporous titanium oxide (ms-TiO_2) precursor, 100 mg TiO_2 paste (30 NR, Dyesol) was dispersed into 850 mg EtOH by ultrasonication for 10 min and then by stirring overnight at room temperature (RT). 1.42 mol of lead iodide (PbI_2, 99.9%, LumTec) was dissolved in 1 mL of mixed solvents of N, N-dimethylformamide (DMF, 99.8%, Merck) and dimethyl sulfoxide (DMSO, 99.8%, Merck) with a volume ratio of 9:1. The PbI_2 solution was heated at 80 °C for 40 min to ensure its complete solution. Thereafter, 1.42 mol of methylammonium iodide

(MAI, 99.8%, LumTec) was mixed with PbI_2 precursor and stirred at RT for 15 min to form $MAPbI_3$ stock solution. To prepare undoped CNTs-based HSM film, 4 mg of CNTs (diameter ~ 8 nm, length ~ 5–20 nm, SkySpring Nanomaterials, Inc.) was dispersed in 1 mL of chlorobenzene (CB, 99.8%, Merck). To synthesize fluorine-doped CNTs (F-doped CNTs) materials, 250 mg of CNTs was added to 100 mL of diluted hydrofluoric (HF) acid solution with different concentrations (0, 0.3, 0.45, 0.6 M) of molar ratio. The obtained mixtures were stirred at room temperature for 24 h before being washed with distilled water until neutral. Then, the washed powders were dried at 100 °C for 24 h and used as F-doped CNT materials in the current study. 4 mg of each of the F-doped CNTs with different levels of doping was dispersed in 1 mL of CB and used as HSM stock solutions.

Solar cell fabrication

A c-TiO_2 layer was formed on the pre-patterned and prewashed FTO substrate by spin coating 40 µL of c-TiO_2 precursor at 4000 rpm for 30 s, followed by annealing at 450 °C for 1 h. To prepare the ms-TiO_2 layer, 60 µL of m-TiO_2 precursor was spin coated over the c-TiO_2 layer at 3000 rpm for 20 s, followed by heating at 500 °C for 1 h. 60 µL of $MAPbI_3$ stock solution was coated on the m-TiO_2 with a speed of 1000 rpm for 10 s and 6000 rpm for 30 s to fabricate the perovskite layer. During the later spin-coating program, 150 µL of CB anti-solvent was instantly poured on the perovskite layer to complete perovskite formation. To make HSM films, different HSM films were drop cast onto the MAPbI3 layer and dried at 70 °C for 5 min. A 100-nm gold electrode was evaporated on the HSM in high vacuum [44].

Characterization

The absorbance spectra of samples were recorded by a Lambda 950 photo-spectrometer. An FLS920P Edinburgh spectrometer recorded the photoluminescence (PL) spectra of samples. To record cross-sectional FESEM images and EDS of samples, a Mira3-XMU FESEM equipment was used. In addition, to record TEM images of samples, a TEM Philips EM 208S instrument was employed. A PANalytical 80 X-ray machine was used to examine the XRD pattern of the perovskite layer. The FT-IR spectra of samples were recorded using an AVATAR thermometer. The Raman spectra of samples were measured with a TakRam N1-541 TESCAN spectrometer. The *J-V* curves of photovoltaic devices were investigated under simulated sunlight illumination. The PSCs were measured with an active area of 0.08 cm^2. A Solartron 1260 galvanostat was used to measure the electrochemical impedance of perovskite solar cells under short-circuit and simulated sunlight irradiation conditions. The external quantum efficiency (EQE) spectra of PSCs were collected using a calibrated Newport IPCE instrument.

Results and discussion

Doping CNTs with nonmetallic substituents has been deemed a useful approach for enhancing CNTs' performance since it can affect the electrical structure and electrochemical characteristics of the pure carbon nanomaterials [45]. In this work, we report the simple synthesis of fluorine-doped CNTs (F-CNTs) and characterization via FT-IR, EDS, and Raman measurements. Furthermore, it is well known that electrical conductivity, which is associated with the widely delocalized π -electrons in the sidewalls, is critical to the performance of CNTs [46, 47]. C–F bond formation is advantageous in optoelectronics because it preserves the delocalized π-system of fluorine-added CNTs. Figure 1a and b displays the morphologies of pure and F-CNTs, respectively. The identical tubular structure of pure and F-doped CNTs is well seen in TEM images, demonstrating that F loading did not drastically change the morphology of CNTs. Different samples of CNTs were analyzed using Raman spectroscopy in order to examine the structural defects caused by the addition of F. Figure 1c demonstrates the presence of the distinctive D-band (defects from edges, vacancies, and functional groups) and G-band (vibration mode of the sp^2 hybrid C skeleton) at 1332 and 1573 cm^{-1}, respectively. The relative intensities of the D and G bands (I_D/I_G values) are 0.046, 0.034, 0.021, and 0.039 for pristine CNTs, F-CNTs-0.30, F-CNTs-0.45, and F-CNTs-0.60, respectively. The value of I_D/I_G for F-CNT-*x* is lower than that of pure CNT, implying effective modification by fluorination [40]. For the F-doped CNT-*x*, the intensities of D-band and G′-band further decrease, which might be resulted from the improved reduction degree. FT-IR patterns of the F-CNT-*x* (Fig. 1d) reveal an absorption band at

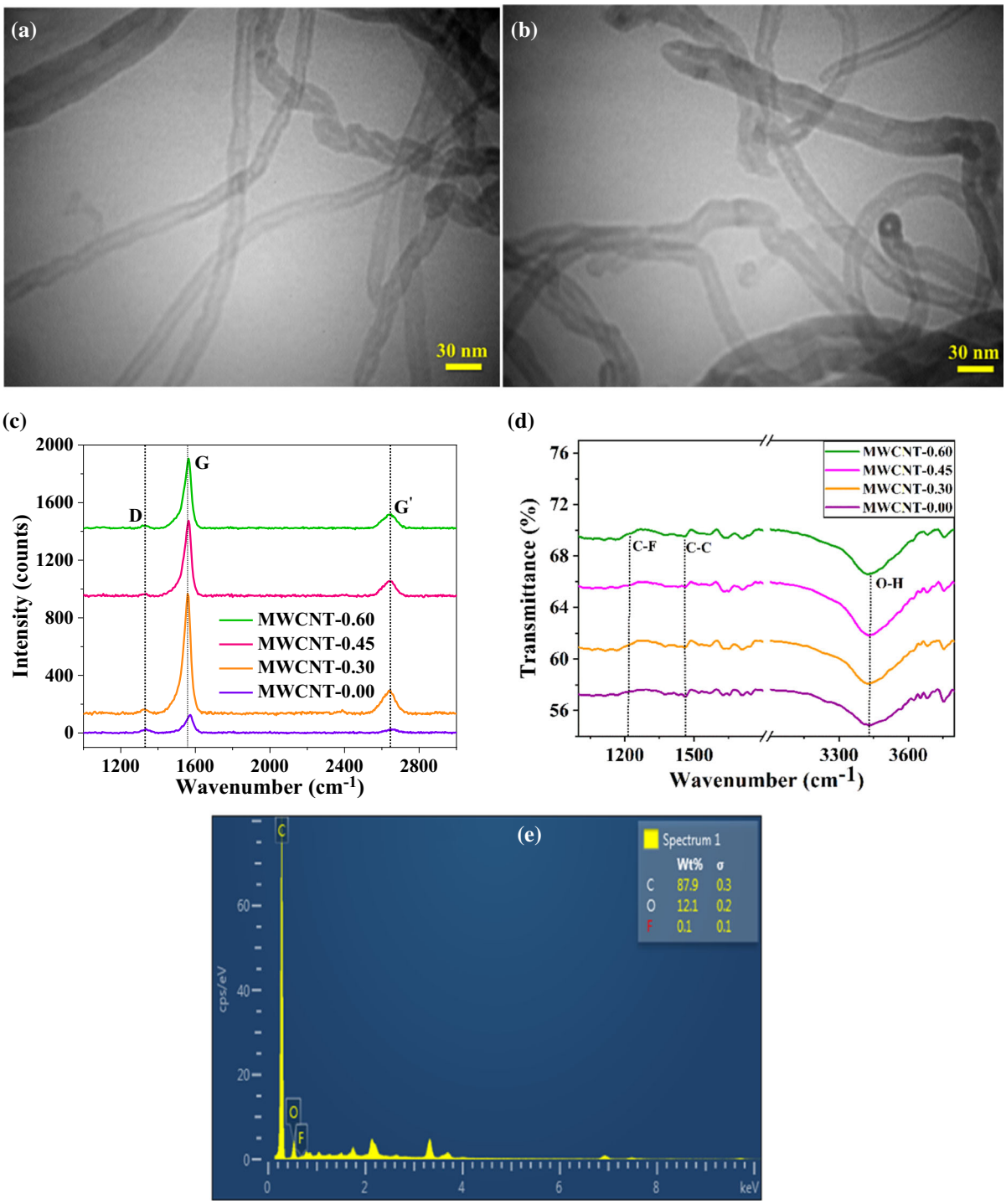

Figure 1 TEM images of **a** pristine CNTs and **b** F-doped CNTs with a 0.45 M HF acid. **c** Raman pattern and **d** FT-IR spectra of CNTs doped with different concentration of HF. **e** EDS spectra of fluorine-doped CNTs with a 0.45 M HF acid.

1221 cm^{-1} attributed to the stretching vibration of covalent C–F bonds, which is in good agreement with the literature [48]. After fluorinating CNTs, the band attributed to the C=C bond weakens, while the hydroxyl O–H bond strengthens. It has been established by analysis of the FT-IR spectroscopy of F-CNT-x that fluorine doping took place predominately on the CNT surface. Elemental atomic composition analysis employing EDS revealed the

existence of carbon, oxygen, and fluorine, as demonstrated in Fig. 1e.

Figure 2a displays the absorption spectrum of a $CH_3NH_3PbI_3$ perovskite coating on an FTO substrate. To be useful as a light harvester, perovskite must have an absorption property in the visible wavelength range, which it achieved. The spectrum also showed the expected absorption shoulders and absorption beginning at 747 and 782 nm, respectively, which agrees with the earlier reported data, and as calculated from Tauc curve (inset of Fig. 2a) yields an energy bandgap of 1.60 eV [49]. As shown, the bandgap of the $MAPbI_3$ film is well matched the sunlight spectrum to efficiently absorb photons and convert them into electrical charges. The bandgap of prepared perovskite is within the optimal range for efficient absorption of visible light, making it a promising absorber for PSCs. The XRD profile of the perovskite deposited on an FTO glass is shown in Fig. 2b. Diffraction peaks at $2\theta = 14.1°$, 28.4°, and 31.8°, correlated to the (110), (220), and (222) planes, respectively, indicate that the material is polycrystalline and has a tetrahedral geometry, as was previously described [50, 51]. A well-oriented polycrystalline structure in the perovskite can facilitate the transport of charge carriers within the material. The partial reaction between PbI_2 and MAI results in the presence of PbI_2 in the perovskite, as evidenced by the peak at 12.38° in the perovskite pattern.

Figure 3a is a diagram showing the assembly of a CNT-based perovskite solar cell. A 450-nm-thick $MAPbI_3$ film was produced using a one-step anti-solvent technique on a substrate made of FTO/c-TiO_2/ms-TiO_2. When chlorobenzene/CNT-containing HF acid was dropped over the $MAPbI_3$ film, a partial $MAPbI_3$–CNT composite top layer was formed, with a relatively thick $MAPbI_3$ bottom layer (Fig. 3b–c). Partially embedded CNTs facilitated fast hole-electron separation and carrier transfer, which may also reduce recombination and improve carrier conduction [52]. As shown in Fig. 3b, pristine CNT-based CPSC showed balky gaps and cracks at the CNT/perovskite interface, leading to an insufficient connection between the $MAPbI_3$ and HSM, resulting in poor carrier transportation and low CPSC performance [53]. On the other hand, with F-doped CNT-0.45 film (Fig. 3c), CNTs could bridge the $MAPbI_3$ film, forming a seamless interface. The CNT bridging approach forms a hole-electron separation highway in the $MAPbI_3$ film and a charge transport highway in the CNT film, giving rise to a high PCE. Figure 3d displays the *J-V* plots of the best-performing CPSCs with pristine CNTs and F-added CNT-*x* HSMs. The key photovoltaic parameters are described in Table 1. The champion PCE (backward scan) of the F-$CNT_{0.45}$-based devices was 15.29%, with a 14.71% average PCE, exhibiting that high-performance device can be fabricated employing only CNT film as the HSM. The champion PCE of the control devices with pristine CNT film was 13.70% (backward scan). Later in the study, differences in V_{OC} and FF, as well as a slight enhancement in J_{SC}, will be examined in detail to explain why the efficiency of the F-added MWCNT devices varies from that of the pristine CNT devices. According to previous studies, a pristine CNT film has a work function of about 5 eV [54], making it close to the value reported for Spiro-OMeTAD, which is about 5.2 eV [55]. In context of this, it shouldn't be a surprise that the V_{OC} value found is close to the value found in the Spiro-OMeTAD devices [38]. Although it was already known that the CNT film transported holes, our findings show that an additional F dopant significantly boosts

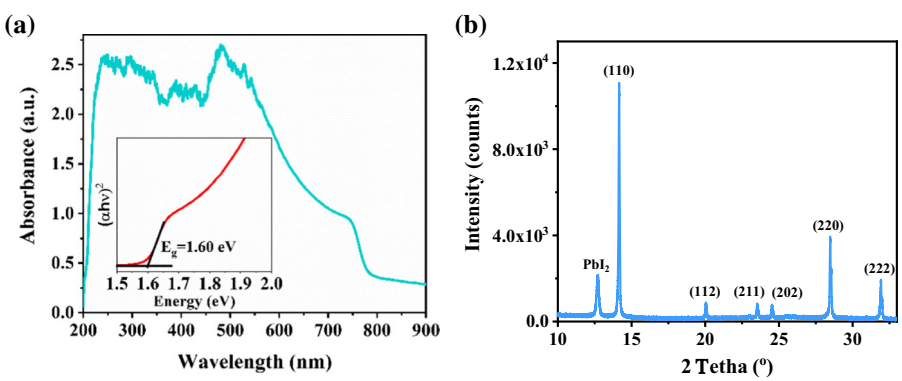

Figure 2 **a** UV–Vis absorbance of $MAPbI_3$ perovskite layer. Inset: the Tauc curve to calculate the energy bandgap. **b** XRD profile of $MAPbI_3$ perovskite layer deposited on FTO glass.

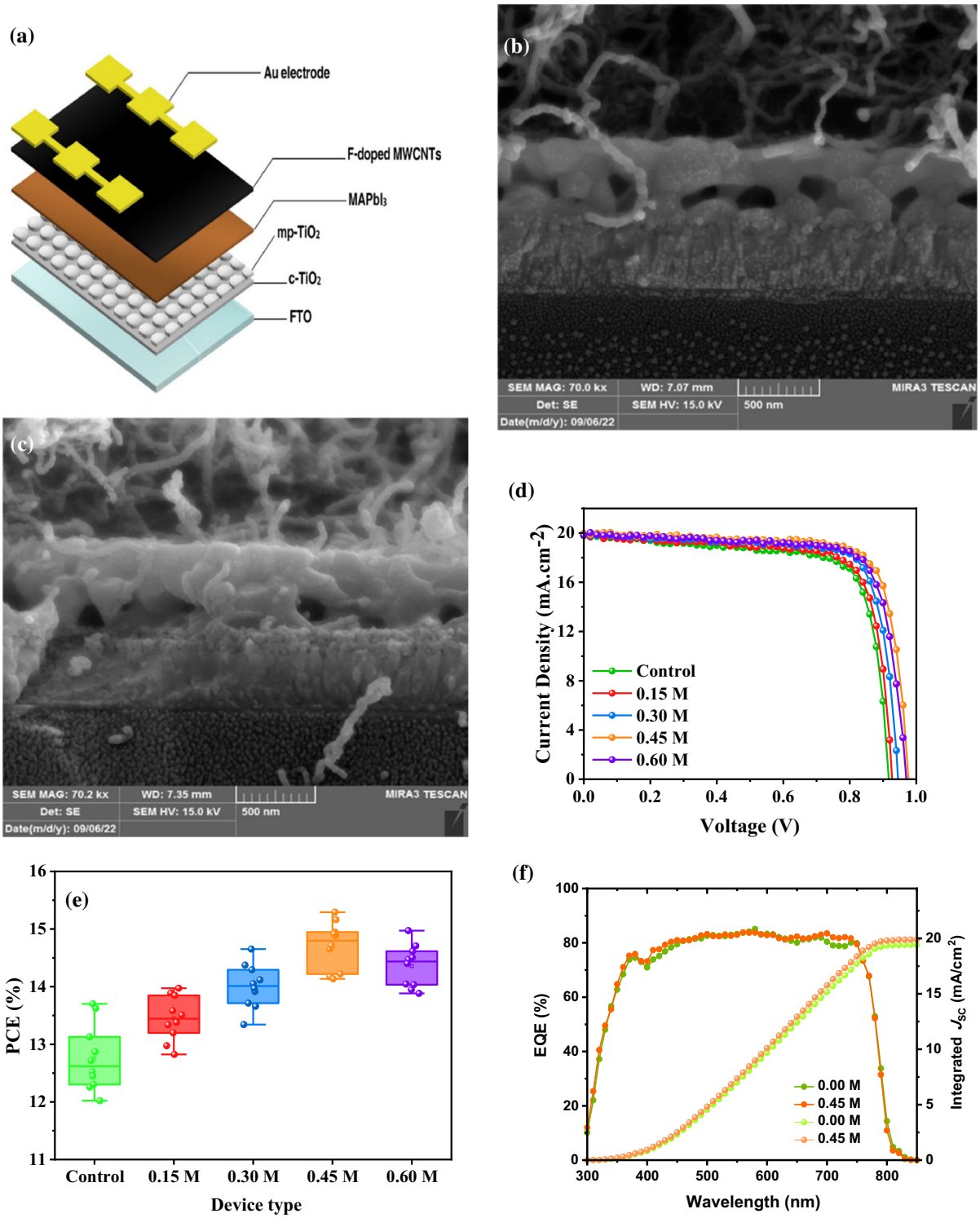

Figure 3 **a** Device illustration of CNT-based perovskite solar cells. Cross-section FESEM micrographs of CPSCs with **b** undoped CNTs film and **c** fluorine-doped CNTs film with 0.45 M HF acid. **d** *J-V* characteristics of the best-performing CPSCs with various CNTs hole-selective materials. **e** PCE statistical distribution of different CPSCs. **f** EQE spectra devices with undoped and 0.45 M HF-modified CNT layers.

Table 1 Photovoltaic parameters of carbon-based PSCs fabricated with different CNTs hole-selective layers

HF Concentration (M)		[a]V_{OC} (V)	[b]J_{SC} (mA/cm^2)	[c]FF (%)	PCE (%)
0.00	Average	0.88 ± 0.02	19.61 ± 0.38	74.09 ± 1.26	12.76 ± 0.54
	Best	0.91	19.82	75.95	13.70
0.15	Average	0.91 ± 0.02	19.64 ± 0.31	75.25 ± 0.54	13.45 ± 0.39
	Best	0.93	19.80	75.89	13.97
0.30	Average	0.93 ± 0.02	19.66 ± 0.19	76 ± 0.49	14.01 ± 0.38
	Best	0.95	19.95	77.31	14.65
0.45	Average	0.95 ± 0.02	19.71 ± 0.22	78.71 ± 0.30	14.71 ± 0.41
	Best	0.97	19.94	79.05	15.29
0.60	Average	0.94 ± 0.02	19.65 ± 0.22	77.57 ± 0.71	14.36 ± 0.37
	Best	0.97	19.82	77.87	14.97

[a]V_{OC} is open-circuit voltage

[b]J_{SC} is short-circuit current density

[c]FF is fill factor

device performance. Furthermore, the fact that the F-CNT provides a higher PCE than pure CNT demonstrates that the F additive also improves the charge collection and transportation in the cells. To further investigate the reproducibility of the CPSCs, the statistics on the PCE several of the different devices based on F-doped CNT-*x* are demonstrated in Fig. 3e. Clearly, the F-CNTs' base CPSCs show small standard deviations and hence enhanced cell reproducibility. Figure 3f also displays the spectrum response of EQE of the C-PSCs treated with HF acid and those not treated. The J_{SC} determined from the *J-V* profiles agrees well with the integrated J_{SC} - estimated from the EQE: 19.42 mA cm^{-2} for the pure-CNT cell and 91.88 mA cm^{-2} for the HF-treated cell.

Using a steady-state PL experiment, we look at how holes are extracted from $MAPbI_3$/HSM multi-layer interfaces. The PL patterns for PSCs formed on FTO glass with different CNT-based HSM films are shown in Fig. 4a. A PL peak appears in the $MAPbI_3$ film at a wavelength of 782 nm, which is in tune with the bandgap of the $MAPbI_3$ material. PL quenching is clearly seen at the CNT/$MAPbI_3$ interface, proving that the CNTs are capable of extracting the holes from the $MAPbI_3$ film. The $MAPbI_3$/F-CNT-0.45 device exhibits greater PL quenching than the CNT-only device, indicating a greater hole collection capacity for the F-CNT layer from the perovskite layer. The emission spectra of F-CNT-based devices also show a slight red shift of around 2.5 nm compared to that of a pristine CNT-based device. This little blue change is indicative of CNTs' ability to passivate the surface-trap state in the $MAPbI_3$ layer [41].

The Nyquist curves (Fig. 4b) were recorded for control and optimized CPSCs under short-circuit state and full-sun irradiation conditions (Z' vs -Z''), where Z' and Z'' are the real and imaginary parts of the device impedance, respectively [56]. The EIS curves were fitted with an equivalent circle as shown in inset of Fig. 4b, and the obtained parameters were listed in Table 2**.** As shown, in the high-frequency region, the arc of CPSC with F-CNT is smaller than that of pristine CNT-based CPSC, implying that the modified CNT film of perovskite suppresses the charge-transfer resistance (R_{ct}) and confirms the role of F-CNT as a hole highway [57]. The value of R_{ct} was reduced 567.4–354.2 Ω after fluorine being doped into CNT layer. Also, series resistance (R_s) showed a notable reduction for F-modified CNT, which provides interface engineering at $MAPbI_3$/CNT and facilitates charge transfer.

Investigations of the long-term stability of CPSCs using CNTs as the HSL that were kept in the dark and at ambient conditions with a humidity of 50% were performed. For an example comparable CPSC device, Fig. 5a shows the variations in photovoltaic performances over the long-term stability experiments. It should be noted that the CNT-based device demonstrated good long-term stability, maintaining 98% of its original efficiency after 100 days. On the other hand, HSL-free CPSC showed fast degradation only after 30 days of testing. The findings highlight that the removal of HSL is critical for the ambient stability of the CPSC device. Humidity degradation of perovskite solar cells is one of their most critical obstacles. Therefore, improving the hydrophobic

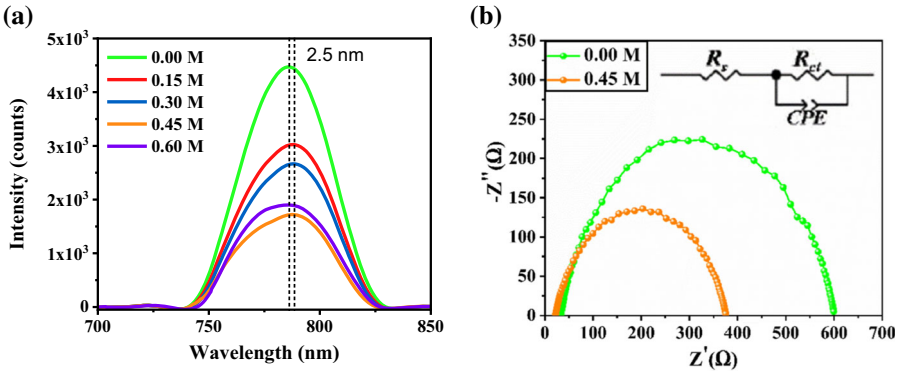

Figure 4 **a** Steady-state PL spectra of carbon-based perovskite solar cells. **b** EIS measurements for control (without F doping) and optimized (with 0.45 F content) devices.

Table 2 The fitted EIS parameters of different carbon-based PSCs

Device name	R_s (ohm)	R_{ct} (ohm)	n	P ($\times 10^{-6}$)
0.00 M	33.1	567.4	0.84	3.2
0.045 M	21.7	354.2	0.81	3.5

behavior of PSCs can increase their resistance against humidity degradation. One technique that can demonstrate the hydrophobic behavior of PSCs is measuring the contact angle of the water droplet, and researchers frequently use this technique [58–60]. Figure 5b and c shows that CNT layers possess high water contact angles. The hydrophobic property of CNTs can efficiently hinder moisture from permeating into the $MAPbI_3$ layer. So, the high stability of the CPSC-based device in the environment should be mostly credited to the hydrophobic CNT.

Fluorine doping of CNT increases the potential of this material for employment as a hole transport layer. As summarized in Table 3, developing F-doped CNT increases the charge-transfer process at the perovskite/CNT interface by reducing the R_{tr} of the PV device, photovoltaic parameters, hydrophobic behavior of CPSCs, and humidity stability of CPSCs.

Table 4 presents an overview of current and pertinent studies related to the utilization of SWCNT or MWCNT in perovskite-based photovoltaic devices. The multifunctional capabilities of carbon nanotubes in solar cells are noteworthy, as they can enhance charge transport, reduce recombination rates, and offer protection for perovskite materials, ultimately resulting in increased stability and efficiency. CNTs possess the potential to serve as additives in HSM for planar and mesoporous PSC architectures.

Conclusion

In summary, we report a CNTs-bridging approach for the preparation of carbon-based $MAPbI_3$ PSCs with considerable efficiency by a cost-effective method. The CNT bridged between the $MAPbI_3$ film

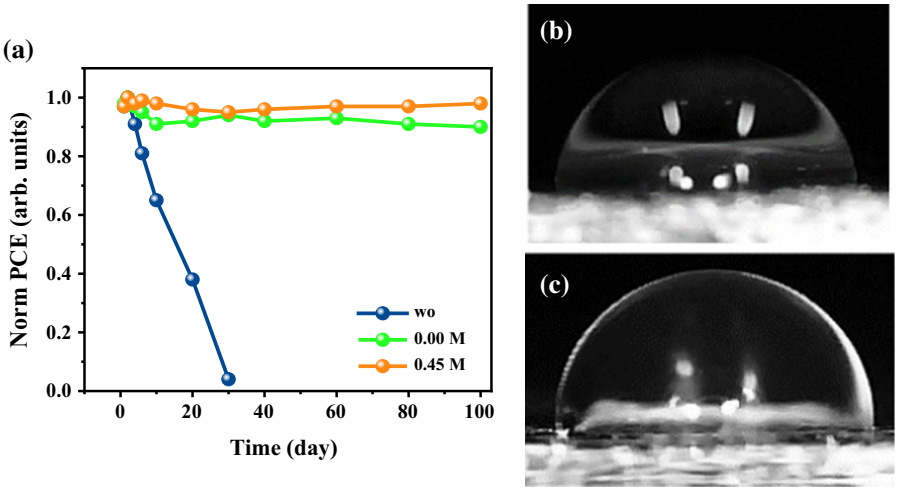

Figure 5 **a** Stability test of different CPSCs at environment with relative humidity of 50% in dark conditions. Contact angle of water droplet on **b** CNT-0.00 and **c** CNT-0.45 layers.

Table 3 Effects of fluorine doping of CNT on photovoltaic and stability of CPSCs

CNT type	Charge transfer	R_{tr}	V_{OC}	J_{SC}	FF	PCE	Hydrophobicity	Stability
Pure CNT	L	H	L	L	L	L	L	L
F-doped CNT	H	L	H	H	H	H	H	H

L and H refer to lower and higher, respectively

Table 4 Comparison between our findings and previously reported studies that utilized CNT as HSMs

Authors	Structure	Study type	V_{OC} (V)	J_{SC} (mA/cm^2)	FF (%)	PCE (%)	Stability
AbdulAlmohsin et al. [61]	ITO/ZnO/$MAPbI_3$/PANI•SWCNT/Au	Simulation	0.56	11.00	30.00	5.00	Not reported
Wei et al.[30]	FTO/TiO_2/$MAPbI_3$/MWCNT	Experimental	0.88	15.60	80.00	12.67	90% stable after 10 days under 20% RH
Wang et al. [25]	FTO/c-TiO_2/ms-TiO_2/$MAPbI_3$/SWCNT/GO/PMMA/Au	Experimental	0.95	19.40	72.00	13.30	95% stable after 10 days under 70–80% RH
Ryu et al.[62]	FTO/c-TiO_2/ms-TiO_2/$Cs_{0.06}(MA_{0.17}FA_{0.83})Pb(I_{0.84}Br_{0.16})_3$/CNT/C	Experimental	1.00	18.97	71.00	13.57	90% stable after 240 min under 80% RH
Zheng et al. [40]	FTO/c-TiO_2/ms-TiO_2/Al_2O_3/$MAPbI_3$/B-MWCNT	Experimental	0.92	21.50	77.00	15.23	98% stable after 80 days in dry air
Wang et al.[52]	FTO/c-TiO_2/ms-TiO_2/$MAPbI_3$•SWCNT/SWCNT•C	Experimental	0.97	22.36	72.22	15.73	100% stable after 90 days under 65 ± 5% RH
Salehi-Abar et al. [19]	FTO/c-TiO_2/ms-TiO_2/$MAPbI_3$/MWCNT/Cr_2O_3/Au	Experimental	1.00	20.80	78.10	16.29	99% stable after 50 days under 40% RH
Mohammed et al. [63]	FTO/ TiO_2/$MAPbI_3$/CNT/Au	Simulation	1.10	19.19	86.62	18.30	Not reported
Kenfack et al. [64]	ITO/Cu_2O/ $MAPbI_3$/SWCNT•[6]CPP/Au	Simulation	1.00	34.65	72.80	25.31	Not reported
This work	FTO/c-TiO_2/mp-TiO_2/$MAPbI_3$/F-CNTs/Au	Experimental	0.97	19.94	79.05	15.29	98% stable after 100 days under 50% RH

C, carbon; MWCNT, multi-walled CNT; c-TiO_2, compact TiO_2; ms-TiO_2, mesoporous TiO_2; SWCNT, single-walled CNT; PANI, polyaniline; P3HT, poly(3-hexylthiophene); Cr_2O_3, chromium(III) oxide; GO, graphene oxide; PMMA, polymethyl methacrylate; B, boron

and back electrodes, leading to improved hole extraction and transport capability and developing an intimate CNT/$MAPbI_3$ interface. Due to such characteristics, an efficiency of 15.29% with an FF of 79.05% was achieved. Moreover, CPSCs based on the CNT layer showed remarkable long-term stability under ambient conditions (50% RH, 25 °C) for about 100 days. The hydrophobic and dense CNT coating protects the $MAPbI_3$ perovskite material from ambient humidity. The current study is a significant step forward in the development of CPSCs, as it has improved their efficiency and stability. This progress could pave the way for the practical use and industrialization of carbon-based PSCs in the future.

Acknowledgements

The authors thank the Researchers Supporting Project number (RSP2023R169), King Saud University, Riyadh, Saudi Arabia for the financial support.

Data availability

Data will be available based on reasonable request.

Declarations

Conflict of interest There is no conflict of interest by any author.

References

[1] Jeong J, Kim M, Seo J, Lu H, Ahlawat P, Mishra A, Yang Y, Hope MA, Eickemeyer FT, Kim M (2021) Pseudo-halide anion engineering for α-FAPbI3 perovskite solar cells. Nature 592(7854):381–385

[2] Guo Z, Jena AK, Kim GM, Miyasaka T (2022) The high open-circuit voltage of perovskite solar cells: a review. Energy Environ Sci 15(8):3171–3222

[3] Gao ZW, Wang Y, Choy WC (2022) Buried interface modification in perovskite solar cells: a materials perspective. Adv Energy Mater 12(20):2104030

[4] Majeed SM, Mohammed MK, Ahmed DS (2022) Efficient and hysteresis-free mixed-dimensional 2D/3D perovskite solar cells using ethyl lactate as a green additive to perovskite precursor solutions. J Mater Chem C 10(43):16480–16491

[5] Humadi MD, Hussein HT, Mohamed MS, Mohammed MK, Kayahan E (2021) A facile approach to improve the performance and stability of perovskite solar cells via FA/MA precursor temperature controlling in sequential deposition fabrication. Opt Mater 112:110794

[6] De Wolf S, Holovsky J, Moon S-J, Loper P, Niesen B, Ledinsky M, Haug F-J, Yum J-H, Ballif C (2014) Organometallic halide perovskites: sharp optical absorption edge and its relation to photovoltaic performance. J Phys Chem Lett 5(6):1035–1039

[7] Noh JH, Im SH, Heo JH, Mandal TN, Seok SI (2013) Chemical management for colorful, efficient, and stable inorganic–organic hybrid nanostructured solar cells. Nano Lett 13(4):1764–1769

[8] Dong Q, Fang Y, Shao Y, Mulligan P, Qiu J, Cao L, Huang J (2015) Electron-hole diffusion lengths > 175 μm in solution-grown CH3NH3PbI3 single crystals. Science 347(6225):967–970

[9] Stranks SD, Eperon GE, Grancini G, Menelaou C, Alcocer MJ, Leijtens T, Herz LM, Petrozza A, Snaith HJ (2013) Electron-hole diffusion lengths exceeding 1 micrometer in an organometal trihalide perovskite absorber. Science 342(6156):341–344

[10] Snaith HJ (2013) Perovskites: the emergence of a new era for low-cost, high-efficiency solar cells. J Phys Chem Lett 4(21):3623–3630

[11] Kareem SH, Elewi MH, Naji AM, Ahmed DS, Mohammed MK (2022) Efficient and stable pure α-phase FAPbI3 perovskite solar cells with a dual engineering strategy: additive and dimensional engineering approaches. Chem Eng J 443:136469

[12] Kadhim MJ, Mohammed MK (2023) Fabrication of efficient triple-cation perovskite solar cells employing ethyl acetate as an environmental-friendly solvent additive. Mater Res Bull 158:112047

[13] Jiang N, Zheng Z, Qin C, Liang R, Li Z, Ye Z, Zhu L (2023) Enhanced power conversion efficiency of perovskite solar cells using dopant-free carbon nanotubes-Spiro-OMeTAD. Ceram Int 49(6):9502–9511

[14] Lou Q, Lou G, Guo H, Sun T, Wang C, Chai G, Chen X, Yang G, Guo Y, Zhou H (2022) Enhanced efficiency and stability of n-i-p perovskite solar cells by incorporation of fluorinated graphene in the Spiro-OMeTAD hole transport layer. Adv Energy Mater 12(36):2201344

[15] Shen Y, Deng K, Li L (2022) Spiro-OMeTAD-based hole transport layer engineering toward stable perovskite solar cells. Small Methods 6(11):2200757

[16] Duan M, Hu Y, Mei A, Rong Y, Han H (2018) Printable carbon-based hole-conductor-free mesoscopic perovskite solar cells: from lab to market. Mater Today Energy 7:221–231

[17] Arora N, Dar MI, Akin S, Uchida R, Baumeler T, Liu Y, Zakeeruddin SM, Grätzel M (2019) Low-cost and highly efficient carbon-based perovskite solar cells exhibiting excellent long-term operational and UV stability. Small 15(49):1904746

[18] Fagiolari L, Bella F (2019) Carbon-based materials for stable, cheaper and large-scale processable perovskite solar cells. Energy Environ Sci 12(12):3437–3472

[19] Salehi-Abar P, Ashassi-Sorkhabi H (2023) MWCNT/Cr2O3 nanocomposite as a solution-processed hole transport layer for cost-effective perovskite solar cells with long-term stability. Sol Energy 251:382–391

[20] Guo M, Liu J, Yuan Y, Zhang Z, Yin S, Leng J, Huang N (2020) CNTs/Cf based counter electrode for highly efficient hole-transport-material-free perovskite solar cells. J Photochem Photobiol A 403:112843

[21] Wei X, Li S, Wang W, Zhang X, Zhou W, Xie S, Liu H (2022) Recent advances in structure separation of single-wall carbon nanotubes and their application in optics, electronics, and optoelectronics. Adv Sci 9(14):2200054

[22] Wang J, Zhang R, Xu H, Chen Y, Zhang H, Park N-G (2022) Polyacrylic acid grafted carbon nanotubes for immobilization of lead (II) in perovskite solar cell. ACS Energy Lett 7(5):1577–1585

[23] Wang X, Xu T, de Andrade MJ, Rampalli I, Cao D, Haque M, Roy S, Baughman RH, Lu H (2021) The interfacial shear strength of carbon nanotube sheet modified carbon fiber composites. In: Challenges in mechanics of time dependent materials, proceedings of the 2020 annual conference on experimental and applied mechanics, vol 2. Springer, pp 25–32

[24] Cao D, Malakooti S, Kulkarni VN, Ren Y, Lu H (2021) Nanoindentation measurement of core–skin interphase viscoelastic properties in a sandwich glass composite. Mech Time-Depend Mater 25:353–363

[25] Wang F, Endo M, Mouri S, Miyauchi Y, Ohno Y, Wakamiya A, Murata Y, Matsuda K (2016) Highly stable perovskite solar cells with an all-carbon hole transport layer. Nanoscale 8(23):11882–11888

[26] Kumar A, Singh S, Mohammed MK, Shalan AE (2021) Effect of 2D perovskite layer and multivalent defect on the performance of 3D/2D bilayered perovskite solar cells through computational simulation studies. Sol Energy 223:193–201

[27] Mohammed MK, Al-Azzawi RK, Jasim HH, Mohammed SH, Singh S, Kadhum HH, Kumar A, Sasikumar P, Revathy M, Jabir MS (2022) Adaption of MAPbI3 perovskite with copper phthalocyanine inorganic hole transport layer via nitrosonium tetrafluoroborate additive to enhance performance and stability of perovskite solar cells. Opt Mater 133:112901

[28] Al-Mousoi A, Mehde M, Al-Gebori A (2020) Annealing temperature effects on the performance of the perovskite solar cells. IOP Conf Ser Mater Sci Eng 757:012039

[29] Li Z, Kulkarni SA, Boix PP, Shi E, Cao A, Fu K, Batabyal SK, Zhang J, Xiong Q, Wong LH (2014) Laminated carbon nanotube networks for metal electrode-free efficient perovskite solar cells. ACS Nano 8(7):6797–6804

[30] Wei Z, Chen H, Yan K, Zheng X, Yang S (2015) Hysteresis-free multi-walled carbon nanotube-based perovskite solar cells with a high fill factor. J Mater Chem A 3(48):24226–24231

[31] Luo Q, Ma H, Zhang Y, Yin X, Yao Z, Wang N, Li J, Fan S, Jiang K, Lin H (2016) Cross-stacked superaligned carbon nanotube electrodes for efficient hole conductor-free perovskite solar cells. J Mater Chem A 4(15):5569–5577

[32] Cheng N, Liu P, Qi F, Xiao Y, Yu W, Yu Z, Liu W, Guo S-S, Zhao X-Z (2016) Multi-walled carbon nanotubes act as charge transport channel to boost the efficiency of hole transport material free perovskite solar cells. J Power Sources 332:24–29

[33] Cao D, Malakooti S, Kulkarni VN, Ren Y, Liu Y, Nie X, Qian D, Griffith DT, Lu H (2022) The effect of resin uptake on the flexural properties of compression molded sandwich composites. Wind Energy 25(1):71–93

[34] Habisreutinger SN, Blackburn JL (2021) Carbon nanotubes in high-performance perovskite photovoltaics and other emerging optoelectronic applications. J Appl Phys 129(1):010903

[35] Tiong VT, Pham ND, Wang T, Zhu T, Zhao X, Zhang Y, Shen Q, Bell J, Hu L, Dai S (2018) Octadecylamine-functionalized single-walled carbon nanotubes for facilitating the formation of a monolithic perovskite layer and stable solar cells. Adv Func Mater 28(10):1705545

[36] Habisreutinger SN, Noel NK, Larson BW, Reid OG, Blackburn JL (2019) Rapid charge-transfer cascade through SWCNT composites enabling low-voltage losses for perovskite solar cells. ACS Energy Lett 4(8):1872–1879

[37] Sakthivel P, Karuppiah M, Asaithambi S, Balaji V, Pandian MS, Ramasamy P, Mohammed MK, Navaneethan N, Ravi G (2022) Electrochemical energy storage applications of carbon nanotube supported heterogeneous metal sulfide electrodes. Ceram Int 48(5):6157–6165

[38] Aitola K, Sveinbjörnsson K, Correa-Baena J-P, Kaskela A, Abate A, Tian Y, Johansson EM, Grätzel M, Kauppinen EI, Hagfeldt A (2016) Carbon nanotube-based hybrid hole-transporting material and selective contact for high efficiency perovskite solar cells. Energy Environ Sci 9(2):461–466

[39] Ago H, Kugler T, Cacialli F, Salaneck WR, Shaffer MS, Windle AH, Friend RH (1999) Work functions and surface functional groups of multiwall carbon nanotubes. J Phys Chem B 103(38):8116–8121

[40] Zheng X, Chen H, Li Q, Yang Y, Wei Z, Bai Y, Qiu Y, Zhou D, Wong KS, Yang S (2017) Boron doping of multiwalled carbon nanotubes significantly enhances hole extraction in carbon-based perovskite solar cells. Nano Lett 17(4):2496–2505

[41] Wang G, Liu J, Chen K, Pathak R, Gurung A, Qiao Q (2019) High-performance carbon electrode-based CsPbI2Br inorganic perovskite solar cell based on poly (3-hexylthiophene)-carbon nanotubes composite hole-transporting layer. J Colloid Interface Sci 555:180–186

[42] Lee J, Menamparambath MM, Hwang JY, Baik S (2015) Hierarchically structured hole transport layers of Spiro-OMeTAD and multiwalled carbon nanotubes for perovskite solar cells. Chem Sus Chem 8(14):2358–2362

[43] Ahmed DS, Mohammed MK (2020) Studying the bactericidal ability and biocompatibility of gold and gold oxide nanoparticles decorating on multi-wall carbon nanotubes. Chem Pap 74(11):4033–4046

[44] Mohammed MK, Jabir MS, Abdulzahraa HG, Mohammed SH, Al-Azzawi WK, Ahmed DS, Singh S, Kumar A, Asaithambi S, Shekargoftar M (2022) Introduction of cadmium chloride additive to improve the performance and stability of perovskite solar cells. RSC Adv 12(32):20461–20470

[45] Wang J, Chen S, Quan X, Yu H (2018) Fluorine-doped carbon nanotubes as an efficient metal-free catalyst for destruction of organic pollutants in catalytic ozonation. Chemosphere 190:135–143

[46] Sun X, Song P, Chen T, Liu J, Xu W (2013) Fluorine-doped BP 2000: highly efficient metal-free electrocatalysts for

acidic oxygen reduction reaction with superlow H_2O_2 yield. Chem Commun 49(87):10296–10298

[47] Mohammad MR, Ahmed DS, Mohammed MK (2020) ZnO/Ag nanoparticle-decorated single-walled carbon nanotubes (SWCNTs) and their properties. Surf Rev Lett 27(03):1950123

[48] Sun C, Feng Y, Li Y, Qin C, Zhang Q, Feng W (2014) Solvothermally exfoliated fluorographene for high-performance lithium primary batteries. Nanoscale 6(5):2634–2641

[49] Noori DA, Behjat A, Dehghanipour M (2023) Operational stability study of hole transport-free perovskite solar cells using lithium fluoride in electron transport layer. J Mater Sci Mater Electron 34(7):592

[50] Ahmed DS, Mohammed BK, Mohammed MK (2021) Long-term stable and hysteresis-free planar perovskite solar cells using green antisolvent strategy. J Mater Sci 56(27):15205–15214

[51] Kadhim AK, Mohammad MR, Abd Ali AI, Mohammed MK (2021) Reduced graphene oxide/Bi2O3 composite as a desirable candidate to modify the electron transport layer of mesoscopic perovskite solar cells. Energy Fuels 35(10):8944–8952

[52] Wang Y, Zhao H, Mei Y, Liu H, Wang S, Li X (2018) Carbon nanotube bridging method for hole transport layer-free paintable carbon-based perovskite solar cells. ACS Appl Mater Interfaces 11(1):916–923

[53] Wang Y, Rho W-Y, Yang H-Y, Mahmoudi T, Seo S, Lee D-H, Hahn Y-B (2016) Air-stable, hole-conductor-free high photocurrent perovskite solar cells with CH3NH3PbI3–NiO nanoparticles composite. Nano Energy 27:535–544

[54] Jeon I, Chiba T, Delacou C, Guo Y, Kaskela A, Reynaud O, Kauppinen EI, Maruyama S, Matsuo Y (2015) Single-walled carbon nanotube film as electrode in indium-free planar heterojunction perovskite solar cells: investigation of electron-blocking layers and dopants. Nano Lett 15(10):6665–6671

[55] Zhou H, Chen Q, Li G, Luo S, Song T-B, Duan H-S, Hong Z, You J, Liu Y, Yang Y (2014) Interface engineering of highly efficient perovskite solar cells. Science 345(6196):542–546

[56] Behera S, Sahoo P, Mishra L, Mohanty B, Choudhary R (2022) Electrical characterization of CaBi4Ti3ZrO15 ceramic. Ferroelectrics 588(1):18–30

[57] Sidhik S, Velusamy J, De la Rosa E, Pérez-García SA, Ramos-Ortiz G, López-Luke T (2019) Role of carbon nanodots in defect passivation and photo-sensitization of mesoscopic-TiO2 for perovskite solar cells. Carbon 146:388–398

[58] Kumar A, Sayyed M, Singh S, Mohammed MK (2023) Interface engineering of Tin (IV) oxide electron transport layer with Yttrium (III) fluoride for efficient carbon-based perovskite solar cells. Mater Sci Semicond Process 163:107561

[59] Christopoulos E, Elsenety MM, Kaltzoglou A, Stoumpos CC, Gaboardi M, Plaisier JR, Tsipas P, Stathatos E, Vitoratos EG, Dimoulas A (2023) 3D/1D architecture using a 1-Hexyl-3-methylimidazolium lead triiodide interlayer for robust and highly performing perovskite solar cells. ACS Appl Electron Mater 5(4):2093–2105

[60] Hangoma PM, Shin I, Yang HS, Kim D, Jung YK, Lee BR, Kim JH, Kim KH, Park SH (2020) 2D perovskite seeding layer for efficient air-processable and stable planar perovskite solar cells. Adv Func Mater 30(34):2003081

[61] AbdulAlmohsin SM, Tareq DE (2020) Fabrication and simulation of peroviskite solar cells comparable study of CuO and Nano composite PANI/SWCNTS as HTM. AIMS Energy 8(2):169–178

[62] Ryu J, Lee K, Yun J, Yu H, Lee J, Jang J (2017) Paintable carbon-based perovskite solar cells with engineered perovskite/carbon interface using carbon nanotubes dripping method. Small 13(38):1701225

[63] Mohammed MK, Al-Mousoi AK, Singh S, Kumar A, Hossain MK, Salih SQ, Sasikumar P, Pandey R, Yadav AA, Yaseen ZM (2023) Improving the performance of perovskite solar cells with carbon nanotubes as a hole transport layer. Opt Mater 138:113702

[64] Kenfack GMD, Nya FT, Laref A (2023) Novel Perovskite solar cell: Incorporating CNTs and Cu2O as charge carriers transport materials for performance enhancement–opto-electrical modelling. Mater Lett 337:133964

Terms and Conditions

Springer Nature journal content, brought to you courtesy of Springer Nature Customer Service Center GmbH (“Springer Nature”).
Springer Nature supports a reasonable amount of sharing of research papers by authors, subscribers and authorised users (“Users”), for small-scale personal, non-commercial use provided that all copyright, trade and service marks and other proprietary notices are maintained. By accessing, sharing, receiving or otherwise using the Springer Nature journal content you agree to these terms of use (“Terms”). For these purposes, Springer Nature considers academic use (by researchers and students) to be non-commercial.
These Terms are supplementary and will apply in addition to any applicable website terms and conditions, a relevant site licence or a personal subscription. These Terms will prevail over any conflict or ambiguity with regards to the relevant terms, a site licence or a personal subscription (to the extent of the conflict or ambiguity only). For Creative Commons-licensed articles, the terms of the Creative Commons license used will apply.
We collect and use personal data to provide access to the Springer Nature journal content. We may also use these personal data internally within ResearchGate and Springer Nature and as agreed share it, in an anonymised way, for purposes of tracking, analysis and reporting. We will not otherwise disclose your personal data outside the ResearchGate or the Springer Nature group of companies unless we have your permission as detailed in the Privacy Policy.
While Users may use the Springer Nature journal content for small scale, personal non-commercial use, it is important to note that Users may not:

1. use such content for the purpose of providing other users with access on a regular or large scale basis or as a means to circumvent access control;
2. use such content where to do so would be considered a criminal or statutory offence in any jurisdiction, or gives rise to civil liability, or is otherwise unlawful;
3. falsely or misleadingly imply or suggest endorsement, approval , sponsorship, or association unless explicitly agreed to by Springer Nature in writing;
4. use bots or other automated methods to access the content or redirect messages
5. override any security feature or exclusionary protocol; or
6. share the content in order to create substitute for Springer Nature products or services or a systematic database of Springer Nature journal content.

In line with the restriction against commercial use, Springer Nature does not permit the creation of a product or service that creates revenue, royalties, rent or income from our content or its inclusion as part of a paid for service or for other commercial gain. Springer Nature journal content cannot be used for inter-library loans and librarians may not upload Springer Nature journal content on a large scale into their, or any other, institutional repository.
These terms of use are reviewed regularly and may be amended at any time. Springer Nature is not obligated to publish any information or content on this website and may remove it or features or functionality at our sole discretion, at any time with or without notice. Springer Nature may revoke this licence to you at any time and remove access to any copies of the Springer Nature journal content which have been saved.
To the fullest extent permitted by law, Springer Nature makes no warranties, representations or guarantees to Users, either express or implied with respect to the Springer nature journal content and all parties disclaim and waive any implied warranties or warranties imposed by law, including merchantability or fitness for any particular purpose.
Please note that these rights do not automatically extend to content, data or other material published by Springer Nature that may be licensed from third parties.
If you would like to use or distribute our Springer Nature journal content to a wider audience or on a regular basis or in any other manner not expressly permitted by these Terms, please contact Springer Nature at

onlineservice@springernature.com